JAAS

Check for updates

Inter-technique comparison of PIXE and XRF for lake sediments

M. El Ouahabi, [iD] *[a] G. Chêne,[bcd] D. Strivay,[bcd] J. Vander Auwera[e] and A. Hubert-Ferrari[f]

In this paper we describe a validation procedure for the chemical analysis of major elements and some minor elements such as Sr, Cr, Ni, Zn and Zr in heterogeneous geological sediments. The procedure applies two distinct techniques (PIXE and XRF) for the analysis of sediments. In this work an inter-technique comparison of heterogeneous lacustrine sediments from Amik Lake in the vicinity of the Roman city of Antioch (SE, Turkey) was carried out. Dried raw samples and samples with linking powder added were analyzed using PIXE performed at the "Arkeo" beamline of the University of Liège AVF cyclotron and XRF (University of Liège). The aim of this work was to compare PIXE and XRF analysis with set-ups routinely in use in the two laboratories. The purpose was also to determine the best combination of techniques and sample preparation protocols to be applied for heterogeneous sediments and the main elements of interest for each specific technique. The results are in agreement among the two techniques, with discrepancies concerning lighter and minor elements. These differences are mainly related to the texture of the sediments and the intrinsic features of the XRF and PIXE techniques. Major and selected minor elements are sensitive to the grain size and porosity of the samples. However, the accuracy of both XRF and PIXE requires the reduction of the grain size or addition of a linking powder to the sediments to fill the voids in order to increase the intensities of both lighter and minor elements. The results demonstrate the critical importance of sample treatment prior to analysis as well as the necessity of several measurement points and replicates to ensure the accuracy of PIXE results.

1. Introduction

To evaluate the environmental impact in sub-aquatic sediment archives, it is vitally important to know their chemical composition and the way it varies in time and in space. To achieve this, we need providing data which are as reliable and complete as possible.

However, analytical techniques most frequently used to monitor sediments such as classical XRF require time-consuming procedures to sample core sediments, and grinding and sieving to refine powders and analyze samples. Despite the fact that X-ray fluorescence (WDXRF) is a well-established analytical technique for geological samples to determine the composition of rocks and sediments,[1–3] there is still a felt need

[a]University of Liege, Géochimie et Environnement Sédimentaires (AGEs), Department of Geology, Belgium. E-mail: Meriam.ElOuahabi@Uliege.be

[b]University of Liège, Institut de Physique Nucléaire Atomique et de Spectroscopie (IPNAS), Department of Physics, Belgium

[c]University of Liège, SANA "Spectroscopie Atomique et Nucleaire, Archeometrie", Belgium

[d]University of Liège, CEA "Centre Europeen d'Archeometrie", U.R. Art, Archéologie et Patrimoine, Belgium

[e]University of Liege, Department of Geology, Belgium

[f]University of Liege, Department of Physical Geography, Belgium

for novel analytical methods for geological samples that can provide as much detail on the chemical composition of individual samples as fast as possible, while at the same time providing accurate results.

In recent years, PIXE (particle induced X-ray emission) is widely used for determining chemical elements in archaeological artifacts such as glass, pigments and other homogenous samples (*e.g.* ref. 4–6) and is potentially an effective way of determining the detailed chemical composition of lacustrine sediments.

PIXE analysis is sometimes carried out simultaneously with PIGE (proton induced gamma ray emission) analysis specifically for Na, Mg, Al and Si quantification.[7,8] PIXE is well established for homogeneous materials like glass, aerosols, ice cores and dust.[9–11] It was also successfully used for archeological artifacts (*e.g.* glass, ceramic, ivory, and bone materials).[6,10,12] Analysis using PIXE offers a number of advantages, such as a short analysis time, a multi-elemental and non-destructive/non-invasive procedure of measurement, fast processing, the absence of pretreatment and satisfactory accuracy for various materials. Nevertheless, PIXE is less used for geological samples due to their heterogeneity and problems related to matrix effects, which in turn introduce errors in proton stopping power and X-ray attenuation calculations (γ-rays have negligible

This journal is © The Royal Society of Chemistry 2018

J. Anal. At. Spectrom., 2018, 33, 883–892 | 883

attenuation within samples). Specific experimental parameters such as probing beam energy and diameter must be adapted and a prior knowledge of the matrix rough composition and heterogeneity of analyzed sediment samples must be required.[13]

The present study focuses on heterogeneous lacustrine sediments with various grain sizes and variable organic matter content. The overall aim of this work was to compare PIXE and XRF capabilities, to investigate the possible benefits of implementing PIXE in macro-beam 1D scanning mode and to determine the best combination of techniques and sample preparation protocols (raw samples or samples with a linking powder) to be applied for sediments. The ultimate purpose was to constrain the evolution of specific chemical indicators through time in sediments to unravel recent paleoenvironmental changes recorded in the lacustrine sediment deposited in the Amik Plain (southern Turkey), close to the Roman city of Antioch (currently called Antakya).
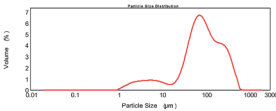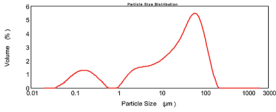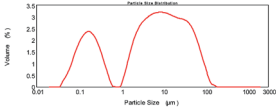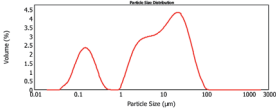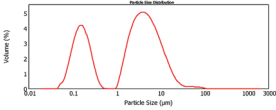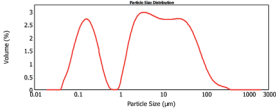
2.   Materials and methods

2.1.   Materials

The study is based on sediment samples collected in Amik Lake (Southern Turkey) at different depths. Sediments are strongly heterogeneous and are mainly the products of the erosion of a wide variety of rocks present in the lake catchment (*i.e.* ophiolitic, ultramafic, volcanic, metamorphic and sedimentary

rocks). Lacustrine sediments have a complex mineralogical composition with more than 15 mineralogical phases due to their geological context. To determine the accuracy of XRF and PIXE devices, samples having variable particle size, texture, organic matter and carbonate content are considered. Six samples were selected at different depth levels (Table 1) after a high-resolution analysis of the first 6 m of sediment deposited. The samples are representative of different sedimentary units deposited over the last 4000 years and show variations in composition, grain-size distribution, carbonate content, magnetic susceptibility and organic matter content. The main characteristics of the selected sediments are summarized in Table 1. Most of the Amik Lake sediments are silty clays, having a small amount of organic matter (∼2–6%) and mostly high carbonate content (∼34–50%). However, shallow sediments (TR1 54 and TR1 106) are more sandy and calcareous due to water saturation (Table 1).

In order to unravel enhanced soil erosion related to human occupation through history, we focus more specifically on variations in Zr, Cr, Ni, and Zn, major elements and Ca/Sr ratio. Zirconium is a reliable index upon which to base quantitative evolution of pedogenic processes in sediments.[13] Cr, Ni and Zn provide insight into the exploitation of ophiolitic rocks and deforestation in the Amanos Mountains close to the study site. The major elements, Si, Ti, Al, Fe, Mn, Mg, Ca, Na and K, are indicative of a terrigenous input in the lake sediments that

Table 1 Grain-size distribution, organic matter and carbonate content of the studied samples. IC: inorganic carbon (loss on ignition at 950 °C for 2 h). OM: organic matter content

Depth (cm)	Samples	Grain size distribution curve	D_{50} (µm)	Clay (%)	Silt (%)	Sand (%)	OM (%)	IC (%)
45	TR1 54		84	0.5	27.1	72.4	2.2	50.5
105	TR1 106		26	16.3	60.0	23.8	2.8	47.1
135	TR1 135		6.8	25.3	68.4	6.3	4.2	46.6
431	T4 70		7.8	23.0	71.7	5.3	3.9	41.7
460	T4 100		2.8	42.3	57.1	0.5	5.5	34.7
476	T4 120		5.1	32.4	60.7	6.8	6.1	34.7

results from the erosion of the surrounding watershed. Finally, because we have a prevalence of carbonate deposition, we use the Ca/Sr ratio as a lake level indicator, seeking in particular to identify the recent drying of the lake and any antecedent immersion of the site.

Samples were taken from the humid core sediments and dried in an oven for 48 h at 40 °C. They were ground and homogenized manually in an agate mortar and divided into two sets. Samples from the first set were ground to less than 20 μm (raw samples), whereas for the second set a linking powder was added. The linking powder is a synthetic carbon polymer used routinely as an additive to dried samples intended for XRF measurements. Both sets were transformed into pellets using a hydraulic press under a pressure of 700 MPa.

2.2. Analytical methods

This inter-technique comparison exercise involves two different devices. The two sets of samples (raw samples and samples with linking powder) were first analyzed by X-ray fluorescence spectrometry using two set-ups.

We first used the X-ray fluorescence spectrometer (Thermo Scientific ARL WDXRF spectrometer) of the University of Liège (Department of Geology, Belgium), equipped with a Rh-tube; the gas used is argon–methane. The quantification of elements was done using UniQuant software which is routinely used for geological sediments. This program is highly effective for analyzing samples for which no standards are available. Major (Si, Ti, Al, Fe, Mn, Mg, Ca, Na and K) and minor elements (S, Cr, Sr, P, Cl, Ni, Ba, Zr, V, Ga, Zn, Co, Sc, Ce, Ag, Cu, Y, Rb, Nb, Cl, P and Rh) were detected and the quantification of the following elements (Si, Ti, Al, Fe, Mn, Mg, Ca, Na, K, Zr, Zn, Ni, Cr and Sr) was performed using UniQuant software without external standards.

A second campaign of measurements was performed on both sets of samples at the Physics Department (ULg) of the Institute of Nuclear, Atomic and Spectroscopy Physics (IPNAS) using a combined PIXE (Proton Induced X-ray Emission) technique. The measurements were performed at the "ARKEO" beamline of the CGR-MEV 520 azimuthally varying field cyclotron of the irradiation facility.

A 3 MeV proton beam, with a diameter of 0.8 mm, is extracted at the end of the beam transport line through a 100 nm thick silicon nitride (Si_3N_4) window and interacts with the samples placed in front of this exit nozzle. Helium gas is flushed in the beam path and in the detection zone to minimize both the energy loss of the probe beam and the absorption of X-rays emitted before collection in the detectors. A total of four spectra are simultaneously collected for each analysis point.

Regarding the PIXE technique, two X-ray spectra are recorded simultaneously using two detectors each of them placed at 45° with respect to the probe beam direction. The first detector, a commercial E2V® Si(Li) detector with a 30 mm² active area and a measured energy resolution of 132 eV @ 5898 keV (Mn Kα), is equipped with an ultra-thin polymer window (AP3.7 Moxtek®) additionally protected from backscattered protons by a magnetic deflector. It is dedicated to the detection of low

energy X-rays (e.g. Na). The second one is a commercial Canberra® UltraLeGe germanium detector with a 50 mm² active area and a measured energy resolution of 160 eV @ 5898 keV (Mn Kα). In addition to its beryllium window, it is equipped with a 100 μm thick aluminum filter in order to absorb preferentially the X-rays emitted by low Z major elements of the matrix. It is therefore dedicated to the detection of higher X-ray energies (6–35 keV) and exhibits enhanced sensitivity to the detection of minor and trace elements of intermediate to high Z elements.

The time of acquisition for an analysis point is typically 10–15 min with a current of 5–10 nA. A specific detection dose control system embedded in the exit nozzle ensures that the same amount of protons is provided to the samples for all analysis points. Before crossing the Si_3N_4 window, a last collimation of the beam is used to intercept its constant fraction. Protons backscattered on the gilded surface of this last collimator are collected in an annular PIPS detector set uphill in the beamline. During measurements, a preset value is fixed for the number of protons scattered and collected in the resulting Rutherford backscattering spectrometry energy spectra, ensuring that the exact same dose is delivered for all analysis points.

Both low and high energy X-ray spectra are then self-consistently treated together using the GUPIX software package[14] and TrauPIXE[15] interface batch mode to obtain elemental weight fractions. The quantification is carried out and ascertained by using Certified Reference geo-Materials standards. The standards are selected in accordance with the typical geochemical composition of the samples. We used well established geo-standards namely Diorite (DR-N) and Basalt (BE-N) provided by the "Service d'Analyse des Roches et Minéraux" (SARM-CRPG-CNRS) to check the accuracy of the quantification procedures after a NIST SRM 610 multi-trace element standard was used to finely calibrate the set-up and determine precisely the charge and geometry factors of the detection set-up. The following elements were detected (Na, Mg, Al, Si, P, S, Cl, K, Ca, Ti, V, Cr, Mn, Fe, Co, Ni, Cu, Zn, Ga, Ge, As, Rb, Sr, Y, Zr, Sn and Sb), and elemental weight concentrations are expressed in oxide forms, as it is generally in sediment studies.

For the purpose of this inter-technique comparison exercise, only the quantification of the following elements (Si, Ti, Al, Fe, Mn, Mg, Ca, Na, K, Zr, Zn, Ni, Cr and Sr) is presented and will be discussed. Moreover, in order to, altogether, estimate elemental concentration errors and understand the dispersion of PIXE results by addressing sample homogeneity issues with respect to the probe size, additional measurements were performed on the sandy sample (TR1 54) by repeating different measurement points at four different locations of the surface of both raw samples and samples with linking powder added.

Finally, PIGE gamma ray spectra are simultaneously recorded in addition, to ensure an accurate quantification of Na generally underestimated using only PIXE. The gamma-ray detector, a commercial Canberra® XtRA, coaxial HPGe germanium device, is placed at 90° with respect to the extracted probe

Table 2 Chemical composition on average of geological standards (DR-N and BE-N) measured using XRF and PIXE devices as well as the standard deviation values computed on measured and references values. Three replicates were measured for each standard. Reference values of the conventional geological standard are also presented in order to compare the reliability of the measured values

	Major elements (%)									Minor elements (ppm)				
	CaO	SiO$_2$	Fe$_2$O$_3$	Al$_2$O$_3$	MgO	K$_2$O	TiO$_2$	MnO	Na$_2$O	Sr	Cr	Ni	Zn	Zr
XRF														
DR-N reference values	7.1	52.9	9.7	17.5	4.4	1.7	1.1	0.2	3.0	400	40	15	145	125
DR-N measured values	6.6	52.6	9.1	14.8	3.3	1.9	1.0	0.2	2.1	1046	62	26	284	358
DR-N SD ($\pm$)	**0.35**	**0.21**	**0.42**	**1.91**	**0.78**	**0.14**	**0.07**	**0.00**	**0.64**	**457**	**15**	**8**	**99**	**165**
BE-N reference values	13.9	38.2	12.8	10.1	13.2	1.4	2.6	0.2	3.2	1370	360	267	120	260
BE-N measured values	12.7	37.4	11.2	10.4	9.2	1.5	2.4	0.2	3.1	3268	567	472	188	634
BE-N SD ($\pm$)	**0.85**	**0.57**	**1.13**	**0.21**	**2.83**	**0.07**	**0.14**	**0.00**	**0.07**	**1342**	**146**	**145**	**48**	**264**
PIXE														
DR-N reference values	7.1	52.9	9.7	17.5	4.4	1.7	1.1	0.2	3.0	400	40	15	145	125
DR-N measured values	6.8	55.0	9.5	18.9	4.1	1.6	1.0	0.2	2.5	311	295	41	129	107
DR-N SD ($\pm$)	**0.21**	**1.48**	**0.14**	**0.99**	**0.21**	**0.07**	**0.07**	**0.00**	**0.35**	**63**	**180**	**18**	**11**	**13**
BE-N reference values	13.9	38.2	12.8	10.1	13.2	1.4	2.6	0.2	3.2	1370	360	267	120	260
BE-N measured values	13.5	40.2	12.3	12.3	12.5	1.4	2.6	0.2	3.1	1177	295	336	120	292
BE-N SD ($\pm$)	**0.28**	**1.41**	**0.35**	**1.56**	**0.49**	**0.00**	**0.00**	**0.00**	**0.07**	**136**	**46**	**49**	**0**	**23**

beam direction. Sodium quantification is carried out following the ^{23}Na(p, p′ γ)^{23}Na reaction occurring in the probed volume and by monitoring the characteristic Na gamma-ray line emitted at 440 keV. The sodium amount measured in the DR-N and BE-N standards is used to calibrate Na quantification for all samples.
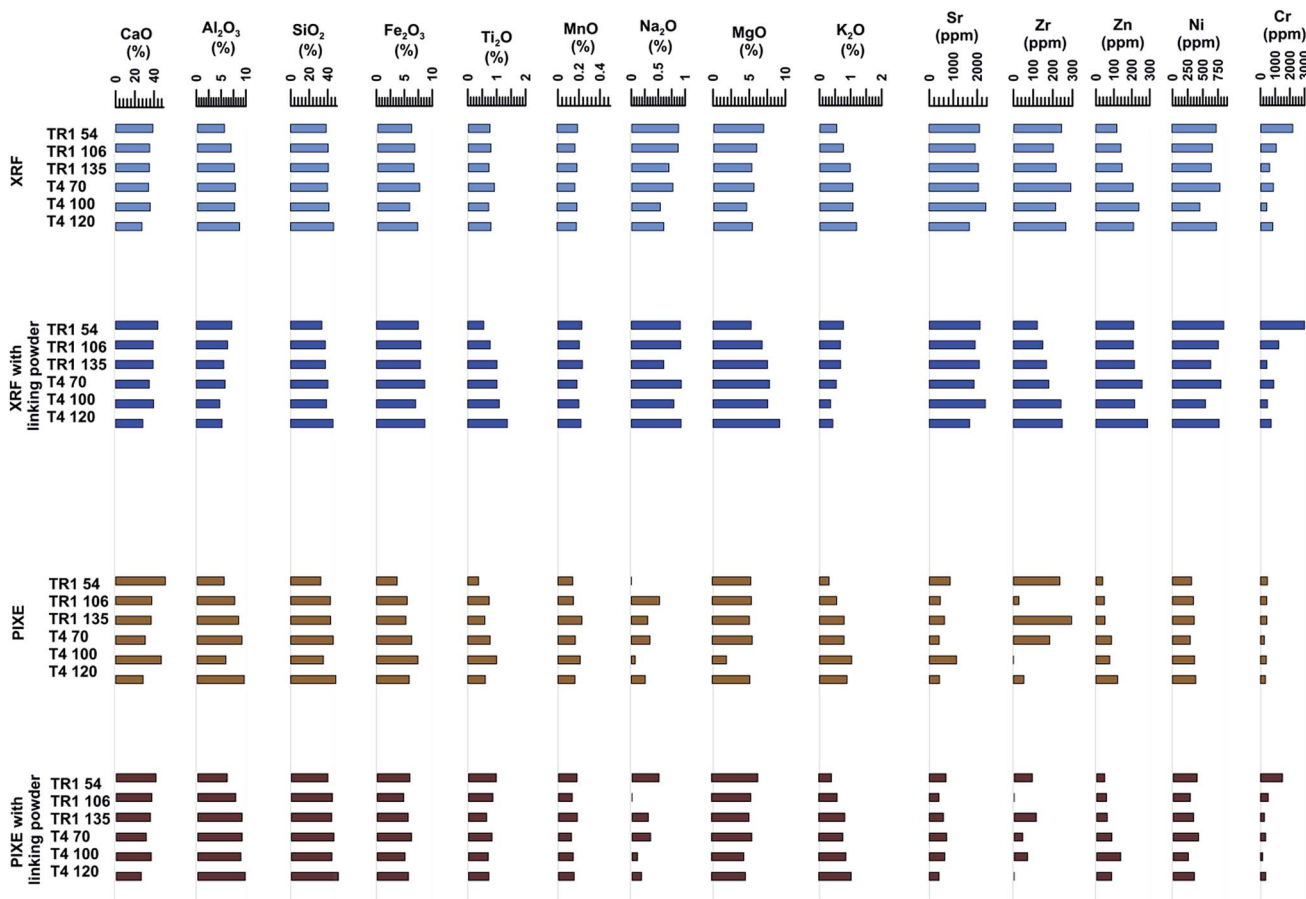

Fig. 1 Selected major and minor element composition of the lake sediments on average at different depths using XRF and PIXE: TR1 54 (54 cm), TR1 106 (106 cm), TR1 135 (135 cm), T4 70 (436 cm), T4 100 (466 cm) and T4 120 (486 cm).

886 | *J. Anal. At. Spectrom.*, 2018, **33**, 883–892

This journal is © The Royal Society of Chemistry 2018

3.   Results and discussion

The inter-technique comparison is first based on geological standards and then on Ca-rich lacustrine samples. This allows us to more clearly identify specific problems linked to heterogeneous sediment samples.

3.1.   Geological standard comparison

Table 2 shows measurements of the geological standard with the two techniques and emphasizes that the reference values and the measured ones are roughly in agreement regarding major and minor elements. K_2O, TiO_2, MnO, Na_2O and CaO show the smallest standard deviation values (SD < 1%) and are slightly underestimated with an XRF device. SiO_2 shows small SD values and is also slightly underestimated. Al_2O_3 is better resolved with PIXE than with XRF, contrary to Si_2O. MgO (up to SD = 2.8% with XRF for BE-N) is systematically underestimated.

Regarding the minor elements, the dispersion is larger. Sr is the least well-resolved with the two techniques due to its high energy. XRF generally provides less well constrained results than PIXE with the ones, especially regarding the BE-N, which contain a large quantity of the selected minor elements. The best constrained elements with PIXE are Zn and Zr.

3.2.   Amik Lake sediments

The average chemical composition taking into account all measurements is Si_2O (37.7 ± 5.7%), CaO (40.1 ± 7.4%), Al_2O_3 (7.6 ± 1.5%), Fe_2O_3 (7.2 ± 1%) and MgO (5 ± 0.9%) (Fig. 1, Tables 3 and 4). Small amounts of Ti_2O (0.8% ± 0.1%), K_2O (1 ± 0.3%), Na_2O (0.5 ± 0.3%) and MnO (0.2%) are also present (Table 3 and Fig. 1). For minor elements, the samples contain highly variable quantities of Sr (1167 ± 748 ppm), Cr (722 ± 770 ppm), Ni (422 ± 283 ppm), Zr (116 ± 69 ppm) and Zn (129 ± 95 ppm) (Table 4 and Fig. 1). In general, all major and selected minor elements were systematically detected by the two devices, but wide differences exist regarding individual oxide quantification of the same sample.

Table 3 Chemical composition (wt%) of the major elements in samples with and without linking powder. (*) Samples mixed with linking powder. The uncertainty of XRF is expressed by standard deviation values (SD) and is computed taking into account the counting statistics of the calibration measurements and the measurement itself (Stat. error) for PIXE

XRF

Samples	CaO	SD	Si_2O	SD	Fe_2O_3	SD	Al_2O_3	SD	MgO	SD	K_2O	SD	Ti_2O	SD	Na_2O	SD	MnO	SD
TR1 54	39.4	0.14	40.3	0.18	6.3	0.03	5.8	0.02	5.9	0.03	0.5	0.00	0.8	0.00	0.9	0.03	0.2	0.00
TR1 54 (*)	44.4	0.05	34.0	0.05	7.6	0.02	5.3	0.02	6.3	0.02	0.6	0.00	1.0	0.03	0.7	0.01	0.2	0.02
TR1 106	35.9	0.37	42.5	0.66	6.9	0.11	7.2	0.06	5.1	0.16	0.7	0.01	0.8	0.01	0.9	0.04	0.2	0.00
TR1 106 (*)	39.4	0.03	37.6	0.01	8.0	0.02	6.8	0.03	5.6	0.01	0.8	0.00	0.9	0.00	0.7	0.02	0.2	0.02
TR1 135	35.7	0.21	42.7	0.22	6.7	0.06	7.9	0.03	4.5	0.04	0.9	0.01	0.7	0.01	0.7	0.02	0.2	0.01
TR1 135 (*)	39.3	0.02	37.7	0.02	7.9	0.01	7.6	0.01	4.9	0.01	1.0	0.00	0.8	0.01	0.5	0.00	0.2	0.02
T4 70	34.7	2.04	41.6	1.76	7.8	0.05	8.1	0.30	4.9	0.27	1.0	0.04	0.9	0.09	0.8	0.07	0.2	0.01
T4 70 (*)	35.2	0.14	40.3	0.19	8.7	0.03	7.8	0.04	5.3	0.40	1.0	0.00	0.9	0.00	0.5	0.00	0.2	0.02
T4 100	36.8	0.26	43.0	0.28	6.1	0.11	7.8	0.02	3.9	0.12	1.0	0.01	0.7	0.03	0.6	0.01	0.2	0.00
T4 100 (*)	39.8	0.03	38.9	0.01	7.1	0.01	7.6	0.01	4.2	0.01	1.1	0.00	0.8	0.01	0.4	0.02	0.2	0.02
T4 120	27.7	0.38	48.6	0.72	7.4	0.18	9.0	0.04	4.5	0.08	1.1	0.02	0.8	0.04	0.6	0.07	0.2	0.01
T4 120 (*)	39.4	0.04	40.3	0.08	6.3	0.01	5.8	0.01	5.9	0.02	0.5	0.01	0.8	0.01	0.4	0.02	0.2	0.02

PIXE

	CaO	Stat. error	Si_2O	Stat. error	Fe_2O_3	Stat. error	Al_2O_3	Stat. error	MgO	Stat. error	K_2O	Stat. error	Ti_2O	Stat. error	Na_2O	Stat. error	MnO	Stat. error
TR1 54	51.8	0.1	31.9	0.2	3.8	0.5	5.7	0.4	5.3	0.5	0.3	2.3	0.4	0.0	0.0	0.0	0.1	3.1
TR1 54(*)	40.0	0.1	38.8	0.1	6.1	0.4	6.2	0.4	6.1	0.5	0.4	1.7	1.0	0.1	0.5	5.5	0.2	2.8
TR1 106	36.4	0.1	42.1	0.1	5.6	0.4	8.0	0.3	5.3	0.5	0.5	1.2	0.8	0.1	0.5	4.6	0.1	2.6
TR1 106(*)	35.8	0.1	43.7	0.1	4.9	0.4	8.0	0.3	5.2	0.5	0.6	1.1	0.9	0.1	0.0	0.0	0.1	2.9
TR1 135	35.8	0.1	42.3	0.1	5.4	0.4	8.8	0.4	5.1	0.6	0.8	1.1	0.6	0.1	0.3	8.8	0.2	2.4
TR1 135(*)	34.4	0.1	42.9	0.2	5.8	0.4	9.3	0.4	5.0	0.6	0.8	1.1	0.7	0.1	0.3	9.7	0.2	3.2
T4 70	29.8	0.1	45.1	0.2	6.4	0.4	9.5	0.4	5.4	0.6	0.8	1.2	0.8	0.1	0.4	8.2	0.2	3.4
T4 70(*)	30.2	0.1	45.2	0.1	6.4	0.4	9.4	0.4	5.3	0.6	0.8	1.1	0.8	0.1	0.3	7.9	0.1	4.1
T4 100	46.0	0.1	34.7	0.3	7.6	0.6	6.1	0.7	1.9	1.8	1.0	1.5	1.0	0.1	0.1	45.3	0.2	5.0
T4 100(*)	35.2	0.1	43.1	0.2	5.2	0.5	9.1	0.4	4.3	0.7	0.9	1.3	0.7	0.1	0.1	28.7	0.1	4.5
T4 120	27.6	0.1	47.9	0.1	6.0	0.4	10.1	0.4	5.1	0.6	0.9	1.1	0.6	0.1	0.3	10.8	0.2	3.4
T4 120(*)	25.2	0.2	50.0	0.1	5.8	0.4	11.1	0.4	4.5	0.7	1.0	0.9	0.7	0.1	0.2	16.0	0.1	3.6

Table 4 Chemical composition of the selected minor elements (ppm) and their error estimation using XRF and PIXE. (*) Samples mixed with linking powder

XRF

Samples	Sr (ppm)	SD	Cr (ppm)	SD	Ni (ppm)	SD	Zn (ppm)	SD	Zr (ppm)	SD
TR1 54	2123	20	2182	58	723	29	251	6	114	1
TR1 54 (*)	2120	13	3191	27	845	17	210	10	121	5
TR1 106	1939	16	1056	39	661	17	208	15	136	15
TR1 106 (*)	1913	13	1243	10	757	14	208	5	149	5
TR1 135	2080	16	599	52	643	23	222	6	143	5
TR1 135 (*)	2089	11	436	11	630	24	214	3	168	4
T4 70	2080	290	854	5	785	40	311	62	203	18
T4 70 (*)	1870	1	905	11	799	11	257	1	179	12
T4 100	2388	25	403	7	457	38	219	9	234	2
T4 100 (*)	2341	13	470	10	543	14	215	10	242	4
T4 120	1694	62	813	30	727	14	274	14	205	18
T4 120(*)	1683	16	726	11	769	11	288	11	247	5

PIXE

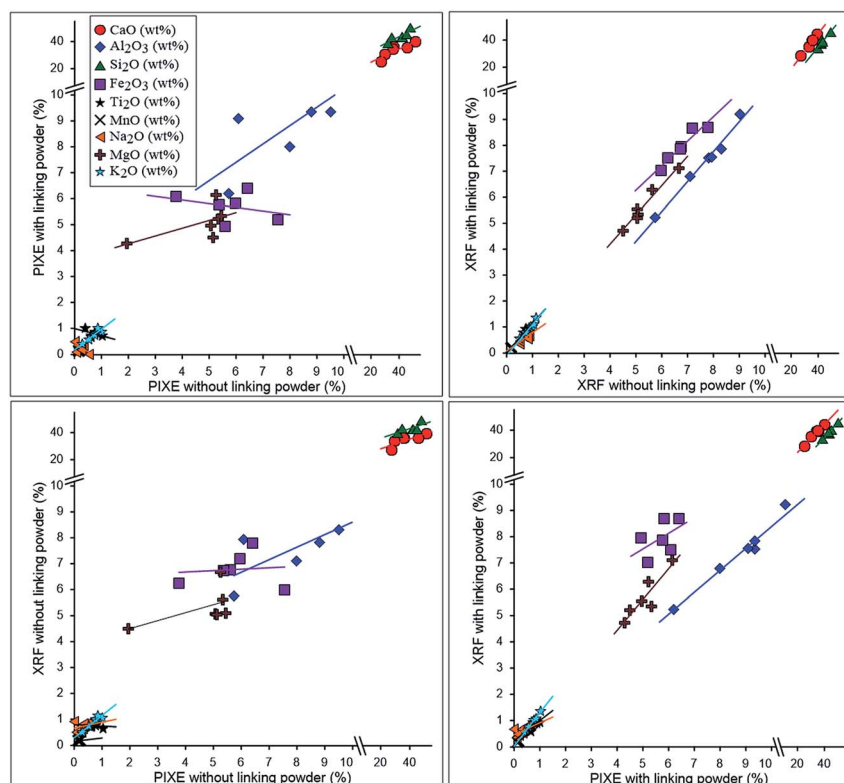|	Sr (ppm)	Stat. error	Cr (ppm)	Stat. error	Ni (ppm)	Stat. error	Zn (ppm)	Stat. error	Zr (ppm)	Stat. error
TR1 54	865	26	469	8	318	18	240	30	37	37
TR1 54 (*)	687	21	1496	3	401	10	94	25	46	84
TR1 106	453	20	424	7	350	10	28	24	47	199
TR1 106 (*)	398	19	525	6	287	11	0	22	56	0
TR1 135	627	25	434	7	362	9	305	29	50	30
TR1 135 (*)	582	23	270	12	342	10	115	27	60	70
T4 70	408	15	265	11	298	10	187	18	85	44
T4 70 (*)	713	13	350	9	424	7	44	16	87	166
T4 100	1125	34	395	13	369	15	0	40	76	0
T4 100 (*)	636	10	148	23	254	13	70	12	137	108
T4 120	419	12	337	9	389	8	53	14	119	135
T4 120 (*)	401	16	355	8	355	7	0	19	85	0

Fig. 2 Correlation graphs between XRF and PIXE measurements for major oxides.

Table 5 Univariate associations (coefficient of determination R^2 is reported) between XRF and PIXE measured in samples with and without linking powder (see Fig. 2 and 3)

	XRF vs. XRF with linking powder	PIXE vs. PIXE with linking powder	PIXE vs. XRF
Major elements			
CaO	0.99	0.98	0.97
Al$_2$O$_3$	0.99	0.98	0.98
Si$_2$O	0.99	0.99	0.98
Fe$_2$O$_3$	0.99	0.94	0.95
Ti$_2$O	0.98	0.87	0.91
MnO	0.99	0.96	0.97
Na$_2$O	0.97	0.24	0.69
MgO	0.99	0.95	0.95
K$_2$O	0.99	0.98	0.98
Minor elements			
Sr	0.99	0.88	0.91
Zr	0.98	0.79	0.60
Zn	0.98	0.87	0.94
Ni	0.99	0.94	0.96
Cr	0.96	0.64	0.78

3.3. Correlation relationships between PIXE and XRF

To test the reliability of the PIXE technique with respect to the XRF one, we performed an inter-comparison of the obtained oxides (Fig. 2 and Table 5). The majority of the major elements show a very strong correlation between PIXE and XRF

measurements (0.98 < R^2 > 0.94). For example, Ti$_2$O shows a strong correlation between PIXE and XRF ($R^2 = 0.91$). Only Na indicates a very weak correlation between PIXE and XRF ($R^2 = 0.69$) because of the attenuation of the scattered signal of this light element (Fig. 1 and Table 3). Na indicates the highest error values (0–45%) for PIXE, while they are between 0 and 0.1 for XRF.

Fig. 2 presents, for all major oxides, the estimated amounts with XRF and PIXE devices. The agreement is fine, but a significant dispersion is visible particularly for Fe$_2$O$_3$, CaO and SiO$_2$, which exhibits high error values for XRF than PIXE. This dispersion is linked to two particular samples, TR1 54 and T4 100, which have the largest CaO content. We use an Al-filter with PIXE to allow for a more accurate determination of light elements that would be masked by a high Ca content; a percentage of CaO greater than 45% impedes an accurate quantification of light elements like Si and Al.

By contrast to the major elements, minor elements show mainly a less strong correlation relationship between PIXE and XRF (Fig. 3 and Table 5). All minor elements are underestimated in PIXE compared to XRF, which was not the case for the geological standard. Zn and Zr amounts are three times lower in PIXE than in XRF. Zn and Zr display more dispersion for XRF than PIXE, having large error values of 12–30 ppm and 0–199 ppm, respectively. This is in agreement with standard values, which suggests an overestimation by XRF (Table 2).

The largest difference is observed regarding Sr, which is strongly attenuated using PIXE. The measurements of the
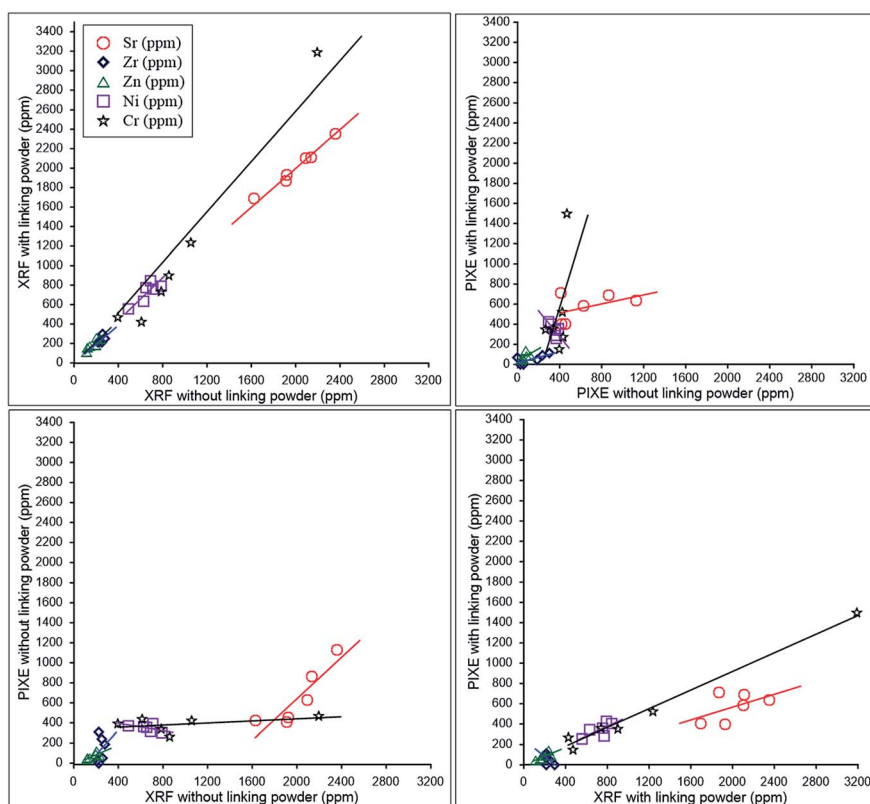

Fig. 3 Correlation graphs between XRF and PIXE measurements for selected minor elements.

geological standards already show that it is overestimated by XRF. Sr indicates slightly highest error values for XRF measurements. The large scattering in Ca and Cr is mainly linked to the less accurate estimate of minor elements with XRF compared to PIXE as evidenced by the geological standards and error values.

3.4. Correlation between raw sediments and samples with linking powder

To assess the influence of the sample porosity on the quantification, we compare the results obtained with raw samples and ones with linking powder (Fig. 2 and 3, Tables 3 and 4). The addition of the linking powder to the samples affects the surface roughness and the porosity. In theory this should improve the radiation scattered from the sample surface by increasing element intensities.[8,16]

For most of the major elements, the oxide composition shows small variation for the same samples with and without linking powder (Fig. 1) and there is a strong correlation between raw samples and samples with linking powder for the two devices (Table 5). The linking powder significantly improved the quantification by converging the measured values using both devices, except for Na_2O by using PIXE ($R^2 = 0.24$). This is in contrast to the standard measurements, suggesting that Na is the most affected by the matrix effect. Furthermore, Na is the only major element indicating a large error up to 45% (Table 3). By adding the linking powder for XRF analyses, K_2O, TiO_2, MnO and MgO show a low dispersion and reduction of error values. These elements show a similar pattern with PIXE. It is well known that with XRF the results are affected by surface roughness effects, thus causing a reduction of concentration when increasing the grain size.[17] The oxide compositions converge to similar results with the two different devices. CaO, which is well constrained (see the geological standard section), shows a different pattern with the two devices. It systematically increases with XRF and decreases with PIXE. As a result, SiO_2 shows a pattern opposite to CaO; it increases with XRF and decreases with PIXE. So, CaO and SiO_2 quantification with XRF and PIXE indicates much more converging results for samples with linking powder. For Al_2O_3, there is also a decrease with XRF and an increase with PIXE, but the overall results are not more coherent. This could be linked to a larger scattering of this light

element with XRF compared to PIXE (see the geological standard, Table 2). We conclude that most of the major elements are sensitive to the characteristics of the surface sample because of the reduction of % error values. In particular regarding PIXE, large changes are observed regarding the two samples with the highest CaO content (TR 54 and T4 100). Regarding minor elements, the difference between XRF and PIXE measurements is striking. For XRF, Ni, Sr, Zr, Cr, and Zn show a good correlation between samples with and without linking powder ($R^2 = \sim 1$). Cr shows a slightly less reliable estimation ($R^2 = \sim 0.96$), despite the diminution of error values with the addition of linking powder (Fig. 3 and Table 5). With regard to the PIXE technique, Ni, Sr and Zr show a moderate to good correlation ($0.94 < R^2 > \sim 0.79$); Cr ($R^2 = 0.64$) indicates a weak correlation and large changes in the amount; Zn displays inconsistent results not being detected in three samples (Tables 4 and 5).

The evaluation of minor elements using PIXE compared to XRF shows a large scattering partly intrinsic to the method as noted with the measurements of the geological standards, but the addition of a linking powder does not change the fact that minor elements are strongly overestimated in XRF compared to PIXE (Fig. 3 and Table 5). The minor elements show different behaviors, which implies that they have a variable sensitivity. Zn, which is the best evaluated element in the geological standard, shows little changes regarding the XRF technique, but using PIXE it is even more underestimated than with raw samples until to be below the detection limit for three samples (Fig. 3). With XRF, Zr, Ni and Cr increase with porosity reduction, and Sr is still scattered. By PIXE, no systematic behavior can be detected, which could again be attributed to the measurement scattering.

The specific scattering observed using the PIXE technique could be linked to two major factors (1) the volume analyzed and (2) the sample heterogeneity. It analyzes a volume much more restricted than XRF. Its beam has an $\sim$0.8 mm size and is completely attenuated after $\sim$0.1 mm, so it is mostly a surface measurement. In contrast, with XRF, we measured a larger reference volume. The types of samples, we studied, also play a crucial role and are different from the geological standards. The geological standards are vitrified and homogeneous, and our sedimentary samples are granular, heterogeneous and porous. We decreased the grain size by grinding the sample and its porosity by using a 10 bar press and then by filling the

Table 6 PIXE results of the TR1 54 sample having a larger particle size. Standard deviation values (SD) were calculated for different measurement points performed on raw samples and ones with linking powder (*). Major elements are in (wt%) and minor elements are in ppm

Samples	CaO	SiO_2	Fe_2O_3	Al_2O_3	MgO	K_2O	TiO_2	MnO	Na_2O	Sr	Cr	Ni	Zn	Zr
TR1 54-1	42.1	37.4	4.7	6.0	7.1	0.3	0.4	0.1	0.5	714	6553	517	65	337
TR1 54-2	39.2	39.4	5.5	6.4	7.1	0.5	0.7	0.1	0.4	872	1092	666	12	146
TR1 54-3	51.8	31.9	3.8	5.7	5.3	0.3	0.4	0.1	0.0	1023	685	405	46	324
TR1 54-4	40.6	38.1	4.4	6.4	7.8	0.3	0.4	0.1	0.6	681	6164	497	61	319
SD ±	**5.71**	**3.31**	**0.72**	**0.32**	**1.09**	**0.08**	**0.13**	**0.02**	**0.28**	**158**	**3166**	**108**	**24**	**91**
TR1 54 (*)-1	40.9	39.5	4.9	6.4	6.1	0.5	0.6	0.2	0.0	691	1469	430	65	392
TR1 54 (*)-2	40.5	37.7	5.8	6.1	6.6	0.4	0.8	0.2	0.5	942	4641	378	137	285
TR1 54 (*)-3	38.3	40.7	5.3	5.9	7.0	0.5	0.7	0.2	0.5	540	2178	574	155	236
TR1 54 (*)-4	38.3	40.3	5.7	6.1	6.8	0.5	1.1	0.2	0.5	555	633	559	62	416
SD ±	**1.41**	**1.34**	**0.41**	**0.23**	**0.39**	**0.06**	**0.18**	**0.01**	**0.25**	**186**	**1727**	**96**	**48**	**86**

890 | *J. Anal. At. Spectrom.*, 2018, **33**, 883–892

This journal is © The Royal Society of Chemistry 2018

residual voids with a linking powder. But given the initial composition of the sediments, the largest particles even after grinding would be quartz grains and shells. We could still have an effect of the initial heterogeneity on the grain size and mineralogy of the samples. To further evaluate its impact regarding PIXE, we carried out additional measurements on the initial coarsest TR 54

sample, which is also the most porous. We perform four additional spot measurements on at sample (Table 6). Al_2O_3, TiO_2, MnO, K_2O, and Na_2O are similar for the two sample types, with a minor improvement of the standard deviation. For CaO, Si_2O and MgO, the quantification is significantly more scattered for raw samples than for samples with linking powder added (Fig. 4).
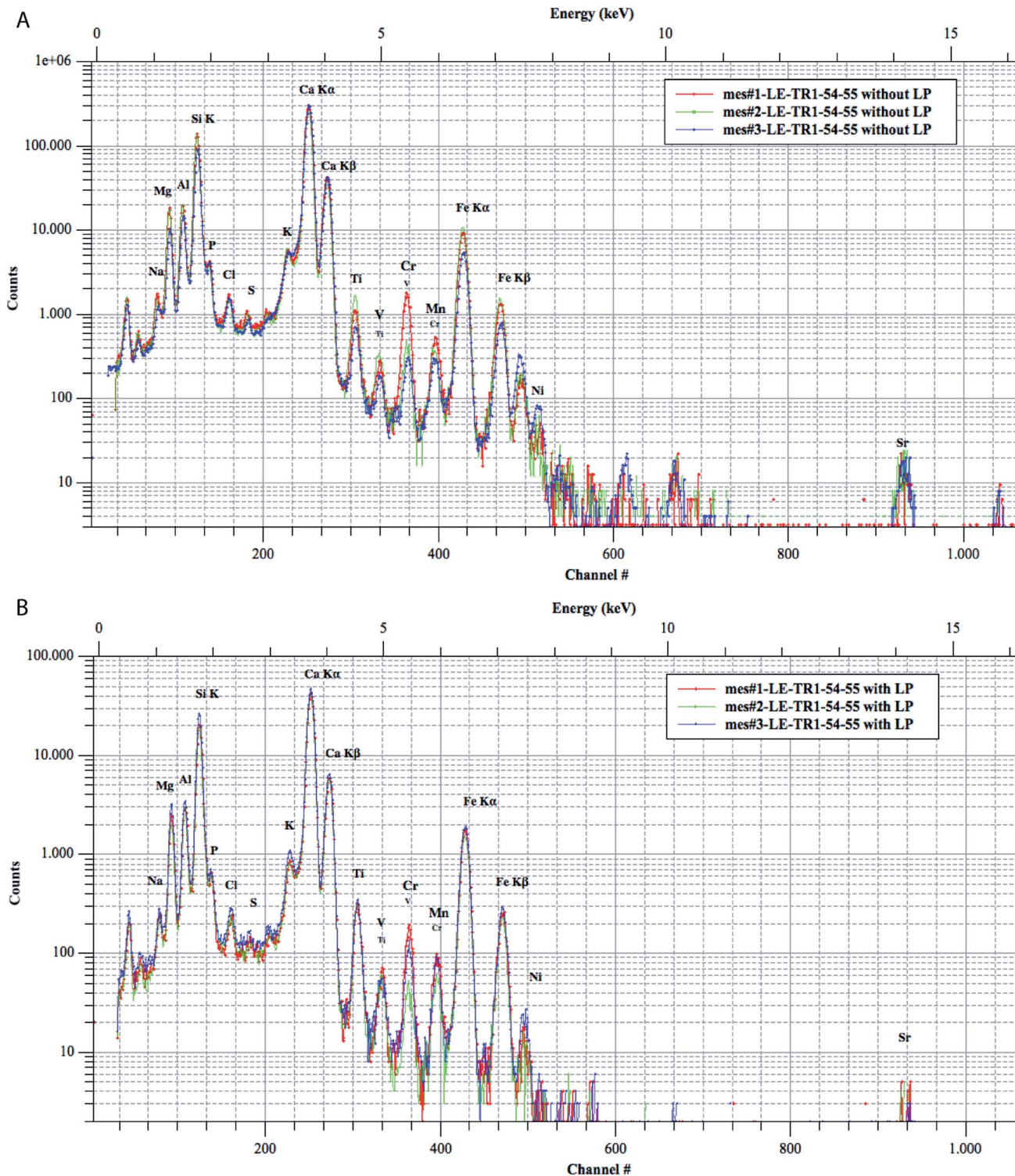

Fig. 4 PIXE spectra of replicates of TR1 54: (A) sample without linking powder (LP) and (B) sample with linking powder.

Regarding the minor elements, the results confirm our previous inferences. We thus conclude that the grain size is a factor predominantly affecting the PIXE results.

The present study suggests that minor elements (Sr, Cr, Ni, Zn and Zr) and the majority of the major elements require a reduction of the porosity of the powdered samples by pressing more than 10 Mbar as well as by adding a linking powder to fill voids in the samples, because the textural properties and grain size of the sediments make a rough surface and then influence fluorescence as well as a more focused induced X-ray emission.

4. Conclusion

The comparison of PIXE and XRF techniques on heterogeneous lake sediments shows a good agreement when a linking powder is used, with discrepancies concerning lighter and minor elements. The differences in the elemental sensitivity for XRF and PIXE are mainly related to the texture of the sediments and the intrinsic features of the XRF and PIXE techniques.

In order to optimize elemental quantification, in the case of heterogeneous lake sediment samples it should be advisable to perform the following points: (1) reduce the grain size of the sample and use a linking powder to optimize fluorescence; (2) do several measurement points to evaluate the accuracy of the results; (3) use PIXE rather than XRF to detect minor elements like Zr, Ni, Zn, and Cr; (4) do elemental mapping of the sample surface only if the elemental changes are larger than the quantification scattering.

Conflicts of interest

There are no conflicts to declare.

Acknowledgements

References

1 M. H. Ramsey, P. J. Potts, P. C. Webb, P. Watkins, J. S. Watson and B. J. Coles, *Chem. Geol.*, 1995, **124**, 1–19.

2 C. P. Swann, *Nucl. Instrum. Methods Phys. Res., Sect. B*, 1995, **104**, 576–583.

3 F. Benyaïch, A. Makhtari, L. Torrisi and G. Foti, *Nucl. Instrum. Methods Phys. Res., Sect. B*, 1997, **132**, 481–488.

4 D. Jembrih-Simbürger, C. Neelmeijer, O. Schalm, P. Fredrickx, M. Schreiner, K. De Vis, M. Mäder, D. Schryvers and J. Caen, *J. Anal. At. Spectrom.*, 2002, **17**, 321–328.

5 J. Pérez-Arantegui, G. Querré and J. R. Castillo, *J. Anal. At. Spectrom.*, 1994, **9**, 311–314.

6 D. Lesigyarski, Ž. Šmit, B. Zlateva-Rangelova, K. Koseva and I. Kuleff, *J. Radioanal. Nucl. Chem.*, 2013, **295**, 1605–1619.

7 C. Boni, E. Cereda, G. M. B. Marcazzan and V. De Tomasi, *Nucl. Instrum. Methods Phys. Res., Sect. B*, 1988, **35**, 80–86.

8 K. H. Janssens, *Modern Methods for Analysing Archaeological and Historical Glass*, Wiley Online Library, 2013.

9 G. Calzolai, M. Chiari, F. Lucarelli, S. Nava, F. Taccetti, S. Becagli, D. Frosini, R. Traversi and R. Udisti, *Nucl. Instrum. Methods Phys. Res., Sect. B*, 2014, **318**, 125–129.

10 C. Heckel, K. Müller, R. White, H. Floss, N. J. Conard and I. Reiche, *Palaeogeography, Palaeoclimatology, Palaeoecology*, 2014, 416, pp. 133–141.

11 F. Marino, G. Calzolai, S. Caporali, E. Castellano, M. Chiari, F. Lucarelli, V. Maggi, S. Nava, M. Sala and R. Udisti, *Nucl. Instrum. Methods Phys. Res., Sect. B*, 2008, **266**, 2396–2400.

12 B. Gómez-Tubío, M. Á. Ontalba Salamanca, I. Ortega-Feliu, M. Á. Respaldiza, F. Amores Carredano and D. González-Acuña, *Nucl. Instrum. Methods Phys. Res., Sect. B*, 2006, **249**, 616–621.

13 O. Valković, M. Jakšić, S. Fazinić, V. Valković, G. Moschini and E. Menapace, *Nucl. Instrum. Methods Phys. Res., Sect. B*, 1995, **99**, 372–375.

14 J. A. Maxwell, W. J. Teesdale and J. L. Campbell, *Nucl. Instrum. Methods Phys. Res., Sect. B*, 1995, **95**, 407–421.

15 L. Pichon, L. Beck, P. Walter, B. Moignard and T. Guillou, *Nucl. Instrum. Methods Phys. Res., Sect. B*, 2010, **268**, 2028–2033.

16 T. O. Richter, S. Van der Gaast, B. Koster, A. Vaars, R. Gieles, H. C. de Stigter, H. De Haas and T. C. van Weering, *Geological Society*, Special Publications, London, 2006, 267, pp. 39–50.

17 I. Liritzis and N. Zacharias, *X-ray fluorescence spectrometry (XRF) in geoarchaeology*, Springer, New York, 2011, pp. 109–142.